J|A|C|S
ARTICLES
Published on Web 07/27/2004

Thermodynamic and Kinetic Stability of Synthetic Multifunctional Rigid-Rod β-Barrel Pores: Evidence for Supramolecular Catalysis

Svetlana Litvinchuk,[†] Guillaume Bollot,[†] Jiri Mareda,[†] Abhigyan Som,[†] Dawn Ronan,[†] Muhammad Raza Shah,[†,§] Philippe Perrottet,[‡] Naomi Sakai,[†] and Stefan Matile*[,†]

Contribution from the Department of Organic Chemistry and Laboratoire de Spectrométrie de Masse, University of Geneva, Geneva, Switzerland

Received March 30, 2004; E-mail: stefan.matile@chiorg.unige.ch

Abstract: The lessons learned from *p*-octiphenyl β-barrel pores are applied to the rational design of synthetic multifunctional pore **1** that is unstable but inert, two characteristics proposed to be ideal for practical applications. Nonlinear dependence on monomer concentration provided direct evidence that pore **1** is tetrameric ($n = 4.0$), unstable, and "invisible," i.e., incompatible with structural studies by conventional methods. The long lifetime of high-conductance single pores in planar bilayers demonstrated that rigid-rod β-barrel **1** is inert and large ($d \approx 12$ Å). Multifunctionality of rigid-rod β-barrel **1** was confirmed by adaptable blockage of pore host **1** with representative guests in planar (8-hydroxy-1,3,6-pyrenetrisulfonate, $K_D = 190$ μM, $n = 4.9$) and spherical bilayers (poly-L-glutamate, $K_D \leq 105$ nM, $n = 1.0$; adenosine triphosphate, $K_D = 240$ μM, $n = 2.0$) and saturation kinetics for the esterolysis of a representative substrate (8-acetoxy-1,3,6-pyrenetrisulfonate, $K_M = 0.6$ μM). The thermodynamic instability of rigid-rod β-barrel **1** provided unprecedented access to experimental evidence for supramolecular catalysis ($n = 3.7$). Comparison of the obtained $k_{cat} = 0.03$ min^{-1} with the $k_{cat} \approx 0.18$ min^{-1} for stable analogues gave a global $K_D \approx 39$ μM^3 for supramolecular catalyst **1** with a monomer/barrel ratio ≈ 20 under experimental conditions. The demonstrated "invisibility" of supramolecular multifunctionality identified molecular modeling as an attractive method to secure otherwise elusive insights into structure. The first molecular mechanics modeling (MacroModel, MMFF94) of multifunctional rigid-rod β-barrel pore hosts **1** with internal 1,3,6-pyrenetrisulfonate guests is reported.

Introduction

The performance of synthetic ion channels and pores depends critically on their thermodynamic and kinetic stability.[1−6] In the case of synthetic multifunctional pores,[3,6] kinetic stability is crucial for control and detection of chemical processes that take place within their confined and oriented internal space. Kinetic stabilities, on one hand, can be assessed from the lifetime of ion channels in conductance measurements: inert pores have a long lifetime; labile ones are short-lived. On the other hand, it is less straightforward to correlate thermodynamic stability and the performance of synthetic multifunctional pores. In general, thermodynamics of self-assembly are reflected in the dependence of fractional supramolecular activity Y on the monomer concentration c_M as described in the Hill equation:[3a,7−10]

$$\log Y = n \log c_M - n \log K_D \qquad (1)$$

Namely, the expected nonlinear dependence characterized by the Hill coefficient n—indicative for the number of monomers needed to form an active supramolecule—is observed only if the concentration c_M of the inactive monomer exceeds the concentration c_B of the active supramolecule clearly (Figure 1).[3a,9,10] A c_M profile following $n > 1$ is, therefore, indicative for unstable active supramolecules. Structural insights beyond n remain, therefore, elusive with ($n > 1$) pores because conventional spectroscopic methods report on inactive monomers. Exergonic self-assembly, on the other hand, can yield functional supramolecules that appear as ($n = 1$) monomers in the Hill equation (1).[3a,10,11] Functional supramolecules characterized by $n < 1$ are metastable intermediates that transform into inactive supramolecular products at high c_M.[3a,10,12] In practice, stable synthetic multifunctional ($n \leq 1$) pores are problematic because they already self-assemble in the media into prepores with hydrophobic outer surfaces that tend to precipitate before interacting with bilayer membranes. Endergonic self-assembly ($n > 1$) from a pool of hydrophilic monomers during incorporation into a bilayer membrane bypasses this solubility problem and can yield pores with excellent characteristics as long as they are inert. As with pore-forming toxins from pathogenic bacteria,[13] derivatives of antifungal natural products such as amphotericin B of practical interest,[5p] or chloride channel mimics for replacement therapy in diseases such as cystic

[†] Department of Organic Chemistry.
[‡] Laboratoire de Spectrométrie de Masse.
[§] Current address: HEJ Research Institute of Chemistry, University of Karachi, Karachi-75270, Pakistan.

10.1021/ja0481878 CCC: $27.50

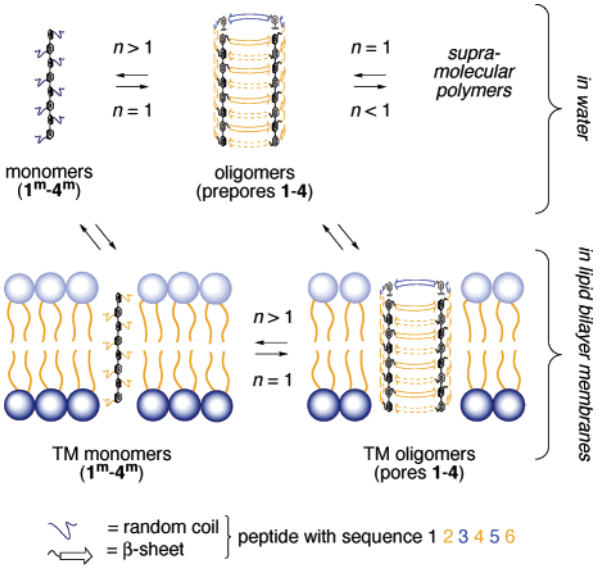

rod	1	2	3	4	5	6	barrel	staves	*n*	unstable	inert	ref
1^m	G	L	K	L	H	L	1	4	4.0	+	+	*this work*
2^m	G	L	H	L	H	L	2	4	1.0	-	-	14,15
3^m	G	L	R	L	H	L	3	4	0.6	-	+	10,16
4^m	G	L	R	W	H	V	4	4	3.9	+	-	10

Figure 1. Multifunctional rigid-rod β-barrels as pores. Endergonic ($n > 1$) and exergonic ($n \leq 1$, eq 1) self-assembly of monomeric rigid-rod molecules $\mathbf{1^m}$−$\mathbf{4^m}$ into aqueous or transmembrane, inert or labile β-barrel prepores or pores **1**−**4** depends on the nature of the amino acid residues at the outer (gold) and inner (blue) barrel surface (single-letter abbreviations; G = −OCH_2CO−). We caution that suprastructures in Figures 1 and 2 are in part speculative representations that are, however, consistent with experimental data and molecular models (see below).

fibrosis,[5e] the ideal synthetic multifunctional pore sensor may, therefore, be an unstable but inert hydrophobic supramolecule that assembles from a pool of hydrophilic precursors in the media. Here, we report the first multifunctional rigid-rod β-barrel pore with these ideal characteristics (i.e., **1**, Figure 1).

Translation of the "secret" of bacterial toxins on how to form perfect pores from hydrophilic precursors to the rational design of "ideal" synthetic multifunctional pores was challenging. Rigid-rod β-barrels **2** with hydrophobic leucines (L) at the outer and catalytic histidines (H) at the inner barrel surface form synthetic multifunctional "HH pores" that are labile (single pore lifetime $\tau = 12$ ms)[14] and stable (c_M profile with $n = 1$).[15] The introduction of internal arginine−histidine dyads gives inert ($\tau > 1$ min)[16] but stable ($n \leq 1$)[10] RH pores **3**. Destabilization by external LWV triads gives unstable ($n = 4$) but labile ($\tau <$ 1 ms) RH pores **4**.[10] Counteranion-mediated stabilization by internal arginines (R)[16,17] and β-sheet destabilization by external tryptophans[10] have been evoked to rationalize these character-

(1) Recent/pertinent reviews/accounts on synthetic ion channels and pores (see also refs 3−6): (a) Koert, U.; Ed. Synthetic Ion Channels. *Bioorg. Med. Chem.* **2004**, *12*, 1277−1350. (b) Gokel, G. W.; Schlesinger, P. H.; Djedovi, N. K.; Ferdani, R.; Harder, E. C.; Hu, J.; Leevy, W. M.; Pajewska, J.; Pajewski, R.; Weber, M. E. *Bioorg. Med. Chem.* **2004**, *12*, 1291−1304. (c) Biron, E.; Otis, F.; Meillon, J.-C.; Robitaille, M.; Lamothe, J.; Van Hove, P.; Cormier, M.-E.; Voyer, N. *Bioorg. Med. Chem.* **2004**, *12*, 1279−1290. (d) Smith, B. D.; Lambert, T. N. *Chem. Commun.* **2003**, 2261−2268. (e) Guo, X.; Szoka, F. C. *Acc. Chem. Res.* **2003**, *36*, 335−341. (f) Koert, U.; Reiss, P. *J. Supramol. Chem.* **2003**, *2*, 29−37. (g) Boon, J. M.; Smith, B. D. *Curr. Opin. Chem. Biol.* **2002**, *6*, 749−756. (h) Savage, P. B.; Li, C.; Taotafa, U.; Ding, B.; Guan, Q. *FEBS Microbiol. Lett.* **2002**, *217*, 1−7. (i) Gokel, G. W.; Mukhopadhyay, A. *Chem. Soc. Rev.* **2001**, *30*, 274−286. (j) Gokel, G. W. *Chem. Eur. J.* **2001**, *7*, 33−39. (k) Matile, S. *Chem. Rec.* **2001**, *1*, 162−172. (l) Cheng, R. P.; Gellman, S. H.; DeGrado, W. F. *Chem. Rev.* **2001**, *101*, 3219−3232. (m) Shum, P.; Kim, J.-M.; Thompson, D. H. *Adv. Drug Delivery Rev.* **2001**, *53*, 273−284. (n) Ranganathan, D. *Acc. Chem. Res.* **2001**, *34*, 919−930. (o) Bong, D. T.; Clark, T. D.; Granja, J. R.; Ghadiri, M. R. *Angew. Chem., Int. Ed.* **2001**, *40*, 988−1011. (p) Sakai, N.; Matile, S. *Chem. Eur. J.* **2000**, *6*, 1731−1737. (q) Kirkovits, G. J.; Hall, C. D. *Adv. Supramol. Chem.* **2000**, *7*, 1−47. (r) Scrimin, P.; Tecilla, P. *Curr. Opin. Chem. Biol.* **1999**, *3*, 730−735. (s) Fyles, T. M. *Curr. Opin. Chem. Biol.* **1997**, *1*, 497−505. (t) Kobuke, Y. *Adv. Supramol. Chem.* **1997**, *4*, 163−210. (u) Koert, U. *Chem. Unserer Z.* **1997**, *31*, 20−26. (v) Gokel, G. W.; Murillo, O. *Acc. Chem. Res.* **1996**, *29*, 425−432. (w) Fyles, T. M.; van Straaten-Nijenhuis, W. F. In *Comprehensive Supramolecular Chemistry*; Reinhoudt, N. D., Ed.; Elsevier: Oxford, 1996; Vol. 10, pp 53−77. (x) Voyer, N. *Top. Curr. Chem.* **1996**, *184*, 1−37. (y) Fuhrhop, J.-H.; Köning, J. *Membranes and Molecular Assemblies: The Synkinetic Approach*; The Royal Society of Chemistry: Cambridge, UK, 1994. (z) Nolte, R. J. M. *Chem. Soc. Rev.* **1994**, *23*, 11−19.

(2) Recent publications on synthetic ion channels and pores (see also refs 4−6, 9−12, and 14−26): (a) Pérez-Hernández, N.; Pérez, C.; Rodríguez, M. L.; Foces-Foces, C.; Tolstoy, P. M.; Limbach, H. H.; Morales, E. Q.; Pérez, R.; Martín, J. D. *Bioorg. Med. Chem.* **2004**, *12*, 1305−1314. (b) Hall, A. C.; Suarez, C.; Hom-Choudhury, A.; Manu, A. N. A.; Hall, C. D.; Kirkovits, G. J.; Ghiriviga, I. *Org. Biomol. Chem.* **2003**, *1*, 2973−2982. (c) Fidzinski, P.; Knoll, A.; Rosenthal, R.; Schrey, A.; Vescovi, A.; Koert, U.; Wiederholt, M.; Strauss, O. *Chem. Biol.* **2003**, *10*, 35−43. (d) Vescovi, A.; Knoll, A.; Koert, U. *Org. Biomol. Chem.* **2003**, *1*, 2983−2997. (e) Eggers, P. K.; Fyles, T. M.; Mitchell, K. D. D.; Sutherland, T. *J. Org. Chem.* **2003**, *68*, 1050−1058. (f) Cameron, L. M.; Fyles, T. M.; Hu, C. *J. Org. Chem.* **2002**, *67*, 1548−1553. (g) De Riccardis, F.; Di Philippo, M.; Garrisi, D.; Izzo, I.; Mancin, F.; Pasquato, L.; Scrimin, P.; Tecilla, P. *Chem. Commun.* **2002**, 3066−3067. (h) Avallone, E.; Izzo, I.; Vuolo, G.; Costabile, M.; Garrisi, D.; Pasquato, L.; Scrimin, P.; Tecilla, P.; De Riccardis, F. *Tetrahedron Lett.* **2003**, *44*, 6121−6124. (i) Arnt, L.; Tew, G. N. *Langmuir* **2003**, *19*, 2404−2408. (j) Zhang, J.; Jing, B.; Regen, S. L. *J. Am. Chem. Soc.* **2003**, *125*, 13984−13987. (k) Murthy, N.; Campbell, J.; Fausto, N.; Hoffman, A. S.; Stayton, P. S. *Bioconjugate Chem.* **2003**, *14*, 412−419. (l) Murthy, N.; Campbell, J.; Fausto, N.; Hoffman, A. S.; Stayton, P. S. *J. Controlled Release* **2003**, *89*, 365−374. (m) Sisson, A. D.; Clare, J. P.; Taylor, L. H.; Charmant, J. P. H.; Davis, A. P. *Chem. Commun.* **2003**, 2246−2247. (n) Epand, R. F.; Umezawa, N.; Porter, E. A.; Gellman, S. H.; Epand, R. M. *Eur. J. Biochem.* **2003**, *270*, 1240−1248. (o) Arvidsson, P. I.; Ryder, N. S.; Weiss, H. M.; Gross, G.; Kretz, O.; Woessner, R.; Seebach, D. *ChemBioChem* **2003**, *4*, 1345−1347. (p) Koulov, A. V.; Lambert, T. N.; Shukla, R.; Jain, M.; Boon, J. M.; Smith, B. D.; Li, H.; Sheppard, D. N.; Joos, J.-B.; Clare, J. P.; Davis, A. P. *Angew. Chem., Int. Ed.* **2003**, *42*, 4931−4933. (q) Schlesinger, P. H.; Djedovic, N. K.; Ferdani, R.; Pajewska, J.; Pajewski, R.; Gokel, G. W. *Chem. Commun.* **2003**, 308−309. (r) Djedovic, N.; Ferdani, R.; Harder, E.; Pajewska, J.; Pajewski, R.; Schlesinger, P. H.; Gokel, G. W. *Chem. Commun.* **2003**, 2862−2863. (s) Schlesinger, P. H.; Ferdani, R.; Pajewska, J.; Pajewski, R.; Gokel, G. W. *New J. Chem.* **2003**, *26*, 60−67. (t) Guo, X.; MacKay, J. A.; Szoka, F. C. *Biophys. J.* **2003**, *84*, 1784−1795. (u) Sidorov, V.; Kotch, F. W.; Kuebler, J. L.; Lam. Y.-F.; Davis, J. T. *J. Am. Chem. Soc.* **2003**, *125*, 2840−2841. (v) Boon, J. M.; Lambert, T. N.; Sisson, A. L.; Davis, A. P.; Smith, B. D. *J. Am. Chem. Soc.* **2003**, *125*, 8195−8201. (w) Sidorov, V.; Kotch, F. W.; Abdrakhmanova, G.; Mizani, R.; Fettinger, J. C.; Davis, J. T. *J. Am. Chem. Soc.* **2002**, *124*, 2267−2278. (x) Sanchez-Quesada, J.; Isler, M. P.; Ghadiri, M. R. *J. Am. Chem. Soc.* **2002**, *124*, 10004−10005. (y) Schlesinger, P. H.; Ferdani, R.; Liu, J.; Pajewska, J.; Pajewski, R.; Saito, M.; Shabany, H.; Gokel, G. W. *J. Am. Chem. Soc.* **2002**, *124*, 1848−1849. (z) Schlesinger, P. H.; Ferdani, R.; Pajewski, R.; Pajewska, J.; Gokel, G. W. *Chem. Commun.* **2002**, 840−841. (aa) Lambert, T. N.; Boon, J. M.; Smith, B. D.; Pérez-Payan, M. N.; Davis, A. P. *J. Am. Chem. Soc.* **2002**, *124*, 5276−5277. (bb) Porter, E. A.; Weisblum, B.; Gellman, S. H. *J. Am. Chem. Soc.* **2002**, *124*, 7324−7330. (cc) Asokan, A.; Cho, M. J. *J. Pharm. Sci.* **2002**, *91*, 903−913. (dd) Tew, G. N.; Liu, D.; Chen, B.; Doerksen, R. J.; Kaplan, J.; Carroll, P. J.; Klein, M. L.; DeGrado, W. F. *Proc. Natl. Acad. Sci. U.S.A.* **2002**, *99*, 5110−5114. (ee) Arnt, L.; Tew, G. N. *J. Am. Chem. Soc.* **2002**, *124*, 7664−7665. (ff) Bandyopadhyay, P.; Bandyopadhyay, P.; Regen, S. L. *J. Am. Chem. Soc.* **2002**, *124*, 11254−11255. (gg) Habaue, S.; Morita, M.; Okamoto, Y. *Macromolecules* **2002**, *35*, 2432−2434. (hh) Habaue, S.; Morita, M.; Okamoto, Y. *Polymer* **2002**, *43*, 3469−3474. (ii) Leevy, W. M.; Donato, G. M.; Ferdani, R.; Goldman, W. E.; Schlesinger, P. H.; Gokel, G. W. *J. Am. Chem. Soc.* **2002**, *124*, 9022−9023. (jj) Vandenburg, Y. R.; Smith, B. D.; Biron, E.; Voyer, N. *Chem. Commun.* **2002**, 1694−1695. (kk) Bandyopadhyay, P.; Bandyopadhyay, P.; Regen, S. L. *Bioconjugate Chem.* **2002**, *13*, 1314−1318. (ll) Raguse, T. L.; Porter, E. A.; Weisblum, B.; Gellman, S. H. *J. Am. Chem. Soc.* **2002**, *124*, 12774−12785. (mm) Shankaramma, S. C.; Athanassiou, Z.; Zerbe, O.; Moehle, K.; Mouton, C.; Bernardini, F.; Vrijbloed, J. W.; Obrecht, D.; Robinson, J. A. *ChemBioChem* **2002**, *3*, 1126−1133. (nn) Ranganathan, D.; Samant, M. P.; Nagaraj, R.; Bikshapathy, E. *Tetrahedron Lett.* **2002**, *43*, 5145−5147. (oo) Sanderson, J. M.; Yazdani, S. *Chem. Commun.* **2002**, 1154−1155.

(3) Reviews of synthetic multifunctional pores: (a) Sakai, N.; Matile, S. *Chem. Commun.* **2003**, 2514−2523. (b) Matile, S. *Chem. Soc. Rev.* **2001**, *30*, 158−167.

(4) The term "pore" is used for systems that transport organic molecules, whereas the term "ion channel" is used for inorganics (all pores are channels, but not all channels are pores).

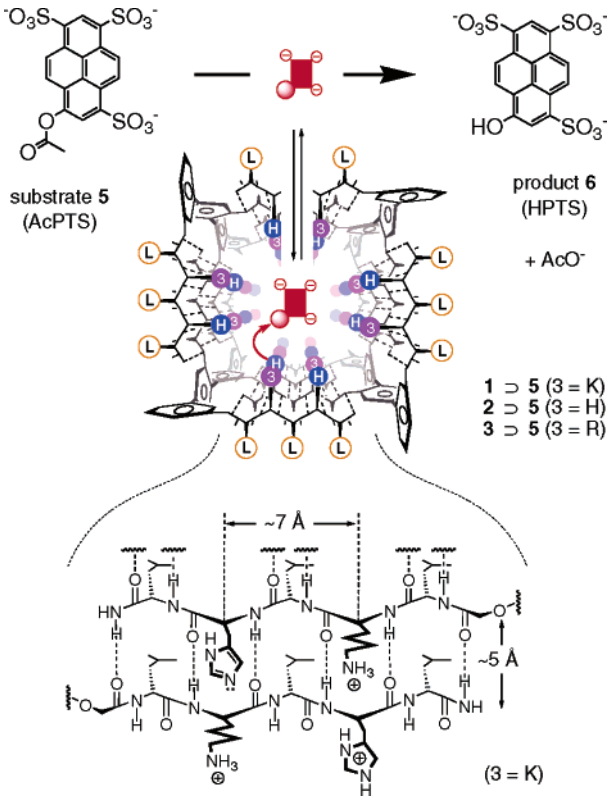

Figure 2. Multifunctional rigid-rod β-barrels as catalysts. Pyrene-1,3,6-trisulfonate substrates like **5** are thought to bind to three proximal cationic amino acid residues (here H, R, or K) at the inner surface of β-barrels **1**−**3** to initiate catalysis at the reactive site consisting of a proximal nucleophilic/basic amino acid residue (here H) and an electrophilic center in the substrate (here an ester). Putative catalyst−substrate complexes **1** ⊃ **5**, **2** ⊃ **5**, and **3** ⊃ **5** include an axial view of (pre)pores **1**−**3** shown in Figure 1.

istics. The only internal residue that served well to both destabilize undesired prepores in the media and reduce the lability of transmembrane rigid-rod β-barrel pores was lysine (K).[15,18,19] Intermediate internal charge repulsion (ICR)[20] between partially protonated internal amines may, therefore, provide general access to the confined and oriented nanospace needed to implement chemistry within synthetic multifunctional pores,[3a,14,21] also on the single-molecule level.[3a,5t−w,21]

With regard to multifunctionality, however, inner surfaces decorated only with partially protonated butylamines are not ideal.[19] Maximal multifunctionality has been identified for pores **2**−**4** with one internal cation to contribute to anion recognition and one internal histidine for catalysis. Over the years, these after all too stable or too labile β-barrel pores have served very well as adaptable supramolecular hosts,[19,22] (enzyme) sensors,[23] and catalysts.[14,21,24−26] For example, the catalysis of the hydrolysis of ester **5** into phenol **6** by HH pores **2** and RH pores **3** was characterized by a transition-state stabilization of more than 50 kJ/mol and a ground-state stabilization of 30−35 kJ/mol (Figure 2).[24] Preorganized ion pairing between the three negative charges of the planar substrate and internal cationic residues was proposed as the supramolecular basis of this quite remarkable example of substrate recognition.

Much indirect evidence in support of the proposed supramolecular recognition is available (independence of catalysis on substrate hydrophobicity,[14] little dependence on partial H/R mutation (**2** versus **3**),[24] strong dependence on ionic strength and pH,[14] and so on). Moreover, several attractive applications such as remote control of catalysis in pore **3** by electrostatic steering with membrane polarization[24] or the introduction of pyrene-1,3,6-trisulfonates as cofactors for a broad variety of otherwise inaccessible substrates[25] became possible assuming

(5) The term "synthetic ion channels and pores" is used for compounds that have abiotic scaffolds (i.e., scaffolds that are not found in biological ion channels and pores) and act in lipid bilayer membranes. This optional definition does not consider ion channels and pores derived from biological peptide scaffolds [(a) Woolley, G. A.; Loughead, T. *Curr. Opin. Chem. Biol.* **2003**, *7*, 710−714. (b) Futaki, S.; Zhang, Y.; Kiwada, T.; Nakase, I.; Yagami, T.; Oiki, S.; Sugiura, Y. *Bioorg. Med. Chem.* **2004**, *12*, 1337−1342. (c) Lougheed, T.; Zhang, Z.; Woolley, G. A.; Borisenko, V. *Bioorg. Med. Chem.* **2004**, *12*, 1343−1350. (d) Scrimin, P.; Tecilla, P.; Tonellato, U.; Veronese, A.; Crisma, M.; Formaggio, F.; Toniolo, C. *Chem. Eur. J.* **2002**, *8*, 2753−2763. (e) Broughman, J. R.; Shank, L. P.; Takeguchi, W.; Schultz, B. D.; Iwamoto, T.; Mitchell, K. E.; Tomich, J. M. *Biochemistry* **2002**, *41*, 7350−7358. (f) Futaki, S.; Fukuda, M.; Omote, M.; Yamauchi, K.; Yagami, T.; Niwa, M.; Sugiura, Y. *J. Am. Chem. Soc.* **2001**, *123*, 12127−12134. (g) Terrettaz, S.; Ulrich, W.-P.; Guerrini, R.; Verdini, A.; Vogel, H. *Angew. Chem., Int. Ed.* **2001**, *40*, 1740−1743. (h) Monoi, H.; Futaki, S.; Kugimiya, S.; Minakata, S.; Yoshihara, K. *Biophys. J.* **2000**, *78*, 2892−2899. (i) Lear, J. D.; Schneider, J. P.; Kienker, P. K.; DeGrado, W. F. *J. Am. Chem. Soc.* **1997**, *119*, 3212−3217. (j) Oiki, S.; Koeppe II, R. E.; Anderson, O. S. *Proc. Natl. Acad. Sci. U.S.A.* **1995**, *92*, 2121−2125. (k) Grove, A.; Mutter, M.; Rivier, J. E.; Montal, M. *J. Am. Chem. Soc.* **1993**, *115*, 5919−5924. (l) Parente, R. A.; Nir, S.; Szoka, F. C. *Biochemistry* **1990**, *29*, 8720−8728. (m) Läuger, P. *Angew. Chem., Int. Ed. Engl.* **1985**, *24*, 905−923], polyester scaffolds [(n) Das, S.; Seebach, D.; Reusch, R. N. *Biochemistry* **2002**, *41*, 5307−5312], natural products [(o) Matsuoka, S.; Matsumori, N.; Murata, M. *Org. Biomol. Chem.* **2003**, *1*, 3882−3884. (p) Yamashita, K.; Janout, V.; Bernard, E.; Armstrong, D.; Regen, S. L. *J. Am. Chem. Soc.* **1995**, *117*, 6249−6253. (q) Muto, Y.; Matsuoka, T.; Kida, A.; Okano, Y.; Kirino, Y. *FEBS Lett.* **2001**, *508*, 423−426. (r) Goudet, C.; Benitah, J.-P.; Milat, M.-L.; Sentenac, H.; Thibaud, J.-B. *Biophys. J.* **1999**, *77*, 3052−3059], artificial membranes [(s) Kimizuka, N. *Curr. Opin. Chem. Biol.* **2003**, *7*, 702−709], engineered biological pores [(t) Bayley, H.; Martin, C. R. *Chem. Rev.* **2000**, *100*, 2575−2594. (u) Luchian, T.; Shin, S.-H.; Bayley, H. *Angew. Chem., Int. Ed.* **2003**, *42*, 1926−1929. (v) Luchian, T.; Shin, S.-H.; Bayley, H. *Angew. Chem., Int. Ed.* **2003**, *42*, 3766−3771], and porous materials [(w) Li, J.; Stein, D.; McMullan, C.; Branton, D.; Aziz, M. J.; Golovchenko, J. A. *Nature* **2001**, *412*, 166−169, and ref 5t].

(6) The term "synthetic multifunctional pores" (SMPs) is used for synthetic pores (ref 5) with additional function(s).

(7) Hille, B. *Ionic Channels of Excitable Membranes*, 2nd ed.; Sinauer: Sunderland, MA, 1992.
(8) Connors, K. A. *Binding Constants*; John Wiley & Sons: New York, 1987.
(9) Stadler, E.; Dedek, P.; Yamashita, K.; Regen, S. L. *J. Am. Chem. Soc.* **1994**, *116*, 6677−6682.
(10) Talukdar, P.; Sakai, N.; Sordé, N.; Gerard, D.; Cardona, V. M. F.; Matile, S. *Bioorg. Med. Chem.* **2004**, *12*, 1325−1336.
(11) Das, G.; Matile, S. *Proc. Natl. Acad. Sci. U.S.A.* **2002**, *99*, 5183−5188.
(12) Das, G.; Ouali, L.; Adrian, M.; Baumeister, B.; Wilkinson, K. J.; Matile, S. *Angew. Chem., Int. Ed.* **2001**, *40*, 4657−4661.
(13) (a) Menestrina, G.; Dalla Serra, M.; Comai, M.; Coraiola, M.; Viero, G.; Werner, S.; Colin, D. A.; Monteil, H.; Prevost, G. *FEBS Lett.* **2003**, *552*, 54−60. (b) Collier, R. J.; Young, J. A. *Annu. Rev. Cell Dev. Biol.* **2003**, *19*, 45−70. (c) Heuck, A. P.; Tweten, R. K.; Johnson, A. E. *Biochemistry* **2001**, *40*, 9065−9073. (d) Abrami, L.; Fivaz, M.; van der Goot, F. G. *Trends Microbiol.* **2000**, *8*, 168−172. (e) Song, L.; Hobaugh, M. R.; Shustak, C.; Cheley, S.; Bayley, H.; Gouaux, J. E. *Science* **1996**, *274*, 1859−1866, see also ref 5e.
(14) Baumeister, B.; Sakai, N.; Matile, S. *Org. Lett.* **2001**, *3*, 4229−4232.
(15) Baumeister, B.; Som, A.; Das, G.; Sakai, N.; Vilbois, F.; Gerard, D.; Shahi, S. P.; Matile, S. *Helv. Chim. Acta* **2002**, *85*, 2740−2753.
(16) Sakai, N.; Sordé, N.; Das, G.; Perrottet, P.; Gerard, D.; Matile, S. *Org. Biomol. Chem.* **2003**, *1*, 1226−1231.
(17) Sakai, N.; Matile, S. *J. Am. Chem. Soc.* **2003**, *125*, 14348−14356.
(18) (a) Baumeister, B.; Sakai, N.; Matile, S. *Angew. Chem., Int. Ed.* **2000**, *39*, 1955−1958. (b) Sakai, N.; Matile, S. *J. Am. Chem. Soc.* **2002**, *124*, 1184−1185. (c) Sakai, N.; Houdebert, D.; Matile, S. *Chem. Eur. J.* **2003**, *9*, 223−232.
(19) Sakai, N.; Baumeister, B.; Matile, S. *ChemBioChem* **2000**, *1*, 123−125.
(20) Internal charge repulsion (ICR): number of charged groups at the inner surface of a pore, increases with pH for acidic residues (e.g., aspartate), decreases with pH for basic residues (e.g., lysine, histidine, and arginine). ICR model: pore activity is maximal at intermediate ICR. See ref 15.
(21) Som, A.; Sakai, N.; Matile, S. *Bioorg. Med. Chem.* **2003**, *11*, 1363−1369.
(22) (a) Das, G.; Onouchi, H.; Yashima, E.; Sakai, N.; Matile, S. *ChemBioChem* **2002**, *3*, 1089−1096. (b) Sordé, N.; Matile, S. *J. Supramol. Chem.* **2002**, *2*, 191−199.
(23) (a) Das, G.; Talukdar, P.; Matile, S. *Science* **2002**, *298*, 1600−1602. (b) Sordé, N.; Das, G.; Matile, S. *Proc. Natl. Acad. Sci. U.S.A.* **2003**, *100*, 11964−11969. (c) Sordé, N.; Matile, S. *Peptide Sci.* **2004**, *76*, 55−65.
(24) Sakai, N.; Sordé, N.; Matile, S. *J. Am. Chem. Soc.* **2003**, *125*, 7776−7777.
(25) Som, A.; Matile, S. *Eur. J. Org. Chem.* **2002**, 3874−3883.
(26) Baumeister, B.; Matile, S. *Macromolecules* **2002**, *35*, 1549−1555.

Scheme 1[a]

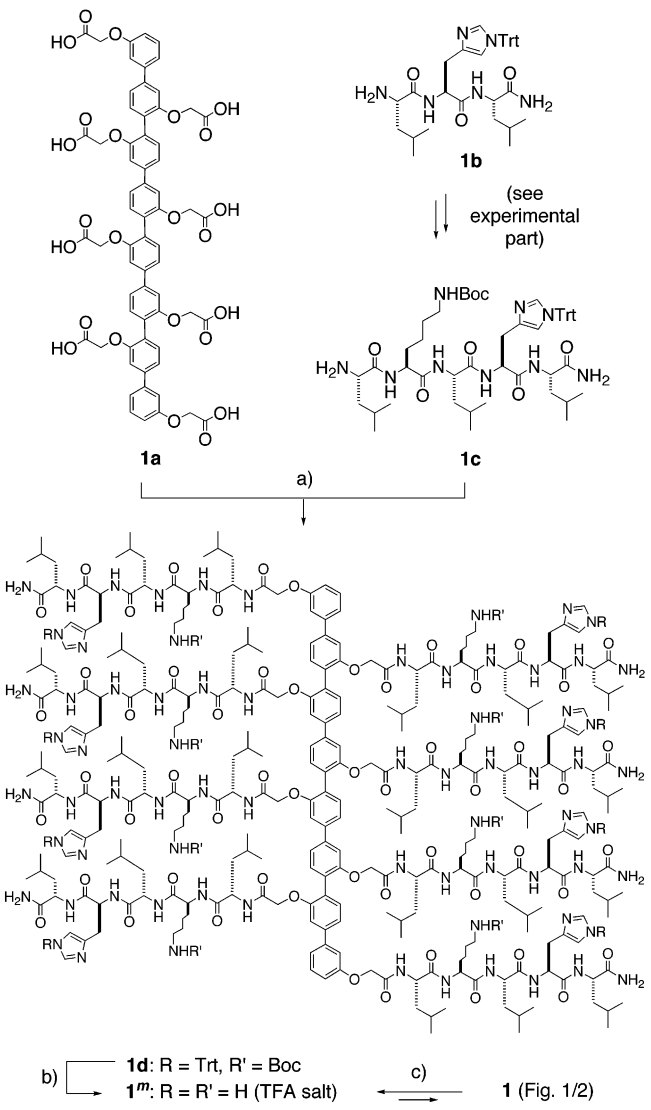

[a] Conditions: (a) HATU, TEA, 22%; (b) TFA, quantitative; (c) self-assembly; see text.

the same supramolecular recognition mechanism. Although all this indirect evidence provides overwhelming support for supramolecular ($n \leq 1$) pores (**2**/**3**) as active hosts and catalysts, there is no direct experimental evidence available that excludes molecular rods (**2**$^{\mathbf{m}}$/**3**$^{\mathbf{m}}$) as active species. In other words, evidence for supramolecular multifunctionality is missing.

The objective of this study was to secure experimental evidence in support of the hypothesis that the "ideal" synthetic multifunctional pore is inert and unstable. To do so, we made and studied rigid-rod β-barrel **1** with internal KH dyads (Figure 1). We report that the rationally designed inertness and instability of synthetic multifunctional pores formed by this new barrel-stave supramolecule provide access to high-conductance pores with long lifetimes without losses in catalytic activity and to experimental evidence for supramolecular catalysis, respectively. These insights on function were, for the first time, simulated on the structural level by molecular modeling.

Results and Discussion

Synthesis of Octakis(*Gla*-Leu-Lys-Leu-His-Leu-NH$_2$)-*p*-Octiphenyl 1$^{\mathbf{m}}$. The peptide−*p*-octiphenyl conjugate **1**$^{\mathbf{m}}$ was synthesized from *p*-octiphenyl **1a** and tripeptide **1b** (Scheme 1). These two intermediates were prepared in an overall 13 steps from commercial starting materials following previously reported procedures.[14] Elongation of tripeptide **1b** into pentapeptide **1c** was as straightforward as expected. The N-terminus of pentapeptide **1c** was reacted with the carboxylate handles along the rigid scaffold of rod **1a** using HATU as coupling reagent, TEA as base, and dimethylformamide (DMF) as the solvent of choice. Deprotection of the resulting conjugate **1d** with TFA gave the target monomer **1**$^{\mathbf{m}}$, which was purified by semi-preparative RP-HPLC. Whereas the electrospray ionization mass spectrometry (ESI MS) of the protected conjugate **1d** gave the expected peaks corresponding to $[M + 8H]^{8+}$, $[M + 7H]^{7+}$, $[M + 6H]^{6+}$, and $[M + 5H]^{5+}$, that of the final conjugate **1**$^{\mathbf{m}}$, measured as TFA salt under denaturing conditions, contained many more peaks. These peaks suggested that the multiply charged $[M + 8H]^{8+}$, $[M + 7H]^{7+}$, $[M + 6H]^{6+}$, and $[M + 5H]^{5+}$ appeared as TFA and H_3PO_4 adducts of various composition (Table 1). This indicated that some TFA anions were replaced by phosphate anions present as "impurities" in the media. Phosphate scavenging by KH-rich rod **1**$^{\mathbf{m}}$ was, however, incomplete. In all cases, counterion-free polycation appeared with highest intensity (entries 1 and 16), and the higher adducts exhibited a preference for TFA rather than for phosphate (entries 34−36 versus 31−33, 28−30 versus 26−27, 23−24 versus 22,

Table 1. Selected Adducts in the ESI Mass Spectra of **1**$^{\mathbf{m}}$ and **3**$^{\mathbf{m}}$ [a]

entry	**1**$^{\mathbf{m}}$ (M = 6035)[b]	**3**$^{\mathbf{m}}$ (M = 6258)[b,c]	H^+ [d]	H_3PO_4[d]	TFA[d]
1	100 (863)	45 (895)	7	0	0
2	90 (877)	50 (909)	7	1	0
3	70 (879)		7	0	1
4	60 (891)	45 (923)	7	2	0
5	65 (893)		7	1	1
6	30 (895)		7	0	2
7		40 (937)	7	3	0
8	40 (907)		7	2	1
9	45 (909)		7	1	2
10	20 (911)		7	0	3
11		20 (951)	7	4	0
12			7	3	1
13			7	2	2
14			7	1	3
15			7	0	4
16	55 (1007)	30 (1044)	6	0	0
17	45 (1023)	100 (1060)	6	1	0
18	25 (1025)		6	0	1
19	40 (1039)	90 (1077)	6	2	0
20	45 (1042)		6	1	1
21	20 (1045)		6	0	2
22		70 (1094)	6	3	0
23	35 (1058)		6	2	1
24	20 (1061)		6	1	2
25			6	0	3
26		45 (1111)	6	4	0
27			6	3	1
28	30 (1077)		6	2	2
29	40 (1080)		6	1	3
30	40 (1083)		6	0	4
31		20 (1128)	6	5	0
32			6	4	1
33			6	3	2
34	35 (1095)		6	2	3
35	45 (1098)		6	1	4
36	25 (1101)		6	0	5

[a] Measured as TFA salts under denaturing conditions (**1**$^{\mathbf{m}}$, CH_3CN/H_2O/AcOH = 74:24:2; **3**$^{\mathbf{m}}$, $CH_3OH/CH_3CN/H_2O$/AcOH = 50:37:12:1). [b] Relative intensity of observed peaks in % (m/z). Consistent with the dynamic nature of counteranion scavenging, the reported adduct patterns were strongly dependent on experimental conditions (such as solvent purity) and fully reproducible as qualitative trends rather than quantitatively. [c] Data from ref 16. [d] Number of adducts (H^+, H_3PO_4, and/or TFA) per monomer.

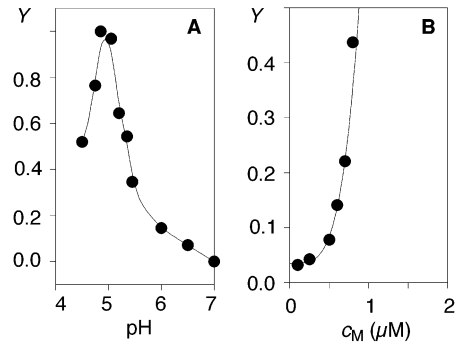

Figure 3. (A) pH profile and (B) c_M profile of rigid-rod β-barrel pore **1**. Fractional activity Y was measured following the increase in ANTS emission during ANTS/DPX efflux from EYPC LUVs after addition of monomer **1**$^{\mathbf{m}}$ ($\approx$250 μM EYPC, 100 mM KCl, 10 mM MES; (A) c_M = 800 nM, (B) pH 5.0). (B) Curve fit to the Hill equation (1), $n = 4.0 \pm 0.3$, solid line.

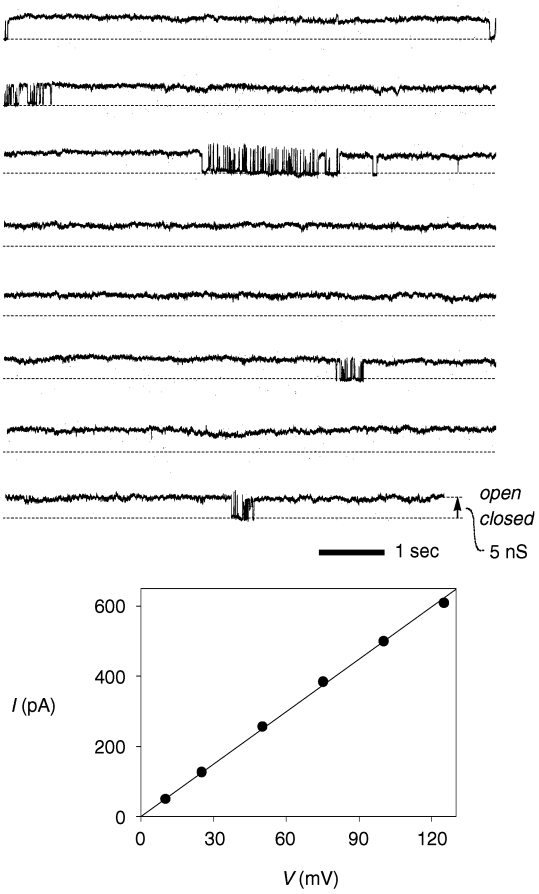

Figure 4. (top) Planar EYPC bilayer conductance in the presence of *p*-octiphenyl **1**$^{\mathbf{m}}$ (4 μM cis, trans at ground) at +25 mV in 2 M KCl. (bottom) Single-channel $I-V$ profile of barrel **1**.

and 8−10 versus 7). This suggested that the phosphate-enriched lower adducts (entries 2, 4, 17, and 19) originate from TFA-rich higher adducts by preferred TFA release rather than from preferred phosphate binding.

This situation with K-rich rod **1**$^{\mathbf{m}}$ was different from that with R-rich rod **3**$^{\mathbf{m}}$, measured as a TFA salt under similar conditions.[16] With oligoarginines, less charged [entry 1 (**1**$^{\mathbf{m}}$) versus entry 17 (**3**$^{\mathbf{m}}$)] and fully "phosphorylated" adducts were observed (entries 2, 4, 7, 11, 17, 19, 22, 26, and 31). Moreover, the phosphate counteranions of R-rich rod **3**$^{\mathbf{m}}$ were not as easily released as with K-rich rod **1**$^{\mathbf{m}}$ [e.g., entry 16 versus entry 17]. This suggested that overall reduced anion (phosphate) scavenging by K-rich rod **1**$^{\mathbf{m}}$ could indeed result in multifunctional pores with the increased internal charge repulsion required for the desired ($n > 1$) behavior (Figures 1 and 2, eq 1).

Rigid-Rod β-Barrels with Internal KH Dyads as Pores. The activity of rigid-rod β-barrels **1** with internal lysine−histidine (KH) dyads as pores was determined in large unilamellar vesicles (LUVs) that were composed of egg yolk phosphatidylcholine (EYPC) and loaded with the fluorescent probe 8-amino-1,3,6-naphthalenetrisulfonate (ANTS) and the quencher *p*-xylene-bis-pyridinium bromide (DPX). After addition of KH rod **1**$^{\mathbf{m}}$, the release of fluorophore or quencher from EYPC LUVs ⊃ ANTS/DPX was readily detectable as an increase of ANTS emission.[10,15] Despite clear disadvantages such as poor sensitivity, the ANTS/DPX assay is, in our hands, ideal for determining c_M and pH profiles of synthetic multifunctional pores because of its minimal dependence on pH and anion/cation selectivity.[10,11,15] According to the ANTS/DPX assay, the activity of KH pore **1** depended strongly on pH. The bell-shaped pH profile showed a sharp maximum at pH 5 (Figure 3A). At pH > 5.0, the activity of KH pore **1** decreased like that of other H-rich pores **2**−**4**.[10,15] At pH < 5.0, the activity of KH pore **1** decreased like that of K-rich rigid-rod β-barrel pores.[15]

The observed pH profile of pore **1**, therefore, suggested that the contributions of internal lysines and histidines to pore function are roughly additive. The ICR model (i.e., maximal pore activity at intermediate internal charge repulsion)[15,20] provided a reasonable explanation for this additivity: pore **1** "implodes" at pH >5.0 because of insufficient ICR from spacially remote lysine residues (intrinsic p$K_a \approx 10.5$) and lacking ICR from histidines (intrinsic p$K_a \approx 6.0$), whereas "explosion" of KH pore **1** at pH <5.0 is—compared to RH pore **3** or HH pore **2**—facilitated by contributions from fully protonated but counter-anion-deficient internal lysines to increasing ICR from internal histidines.

Around optimal pH, the c_M profile of KH pore **1** in EYPC LUVs ⊃ ANTS/DPX was nonlinear (Figure 3B). Fit to the Hill equation (1) gave a Hill coefficient $n = 4.0 \pm 0.3$. As discussed in the Introduction, this ($n > 1$) behavior had three significant implications: (1) the active pore is a supramolecule (i.e., a tetramer—or, less likely, an octamer self-assembling from a stable dimer, a dodecamer self-assembling from a stable trimer, and so on), (2) this active tetramer is *unstable* (Figure 1), and (3) structural studies by conventional methods are not applicable to pore **1** because they will report on the excess inactive monomer **1**$^{\mathbf{m}}$ in the system.

In planar EYPC bilayers with an applied voltage of $V = +25$ mV, a high-conductance pore with long lifetime was observed together with bursts of nearly identical conductance. As in previous reports,[10,18c] we speculated that the labile pores are intermediate to the formation of the inert pores. The mean lifetime of the long-lived single KH pore **1** was $\tau = 14.1$ s (Figure 4). The lifetime of high-conductance pore **1** was, therefore, beyond that of many classical, biological low-conductance ion channels such as gramicidin A. Clearly, the unstable pores formed by rigid-rod β-barrels were as *inert* as expected (Figure 1). In excellent agreement with β-sheet destabilization at high polarization, where strong dipole-potential repulsion may disturb the antiparallel alignment of the backbone amides,[27] the mean lifetime of single pore **1** decreased with

(27) Bainbridge, G.; Gokce, I.; Lakey, J. H. *FEBS Lett.* **1998**, *431*, 305−308.

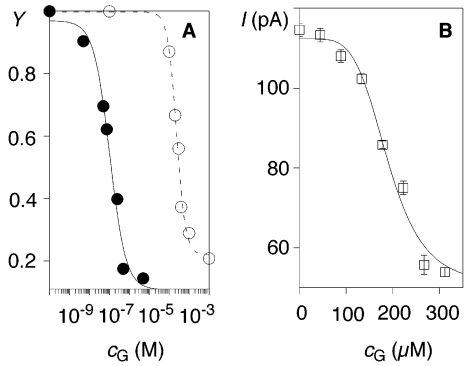

Figure 5. Fractional activity Y of rigid-rod β-barrel pore hosts **1** as a function of concentration c_G of guests such as (A) poly-L-glutamate (filled circles) and ATP (empty circles) in spherical EYPC LUVs ⊃ ANTS/DPX ($V = 0$ mV) and (B) HPTS **6** in planar EYPC bilayers (multichannel current I at $V = +100$ mV, 5 mM MES, 100 mM KCl, pH 5.0) with curve fit to the Hill equation (1).

increasing voltage to a still quite remarkable $\tau = 0.36$ s at $V = +125$ mV.

The current flowing across single pores showed linear voltage dependence within ±100 mV (Figure 4). Such ohmic behavior is characteristic for symmetric β-sheet secondary structures as in biological and rigid-rod β-barrel pores, where the opposing orientation of the backbone amides results in no macrodipole.[3a] A conductance $g = 4.98 \pm 0.05$ nS for the dominant single pore resulted from the slope of this ohmic $I-V$ profile. Elimination of contributions from the resistivity of the recording solution from $g \approx 5$ nS using Hille's equation[7] gave a pore diameter $d_{Hille} = 12$ Å. Different from the underestimates obtained with low-conductance pores, Hille diameters are expected to reflect the internal space of high-conductance pores like **1** quite accurately.[21,28] $d_{Hille} = 12$ Å is the largest Hille diameter found so far for tetrameric rigid-rod β-barrel pores.[3a] It was consistent with minimal counteranion scavenging expected with internal lysine residues and, consequently, maximal internal charge repulsion to stabilize the large, oriented and multifunctional "nanospace" within pore **1**.

Rigid-Rod β-Barrel Pores with Internal KH Dyads as Hosts. To combine molecular translocation with molecular recognition, the activity of synthetic multifunctional pore **1** in spherical EYPC LUVs ⊃ ANTS/DPX was assessed in the presence of increasing concentrations of representative guests. As with RH pore **3** ($K_D = 150$ nM, pH 4.5, $K_D = 45$ nM, pH 5.5),[22b] ANTS/DPX translocation across KH pore host **1** could be efficiently blocked with partially α-helical poly-L-glutamate as a representative guest ($K_D = 105 \pm 27$ nM, pH 5.0, Figure 5A, filled circles). The obtained nanomolar apparent K_D suggested that nearly stoichiometric association obscured an actual $K_D < 150$ nM. The Hill coefficient $n = 1.0 \pm 0.3$ may be indicative for the binding of one polypeptide guest per tetrameric pore host **1**.[29] As with RH pore **4** ($K_D = 82$ μM, pH 6.5),[23c] about 3 orders-of-magnitude higher guest concentrations were required to block KH pore host **1** with ATP (adenosine triphosphate; $K_D = 240 \pm 25$ μM, pH 5.0, Figure 5A, empty circles). The obtained Hill coefficient $n = 2.0 \pm 0.4$ could indicate that binding of two ATP molecules was required to block ANTS/DPX translocation across tetrameric pore host **1**.[29] KH pore **1** could not be blocked with the nonfluorescent pyrene-1,3,6,8-tetrasulfonate (PTS) at detectable concentrations ($K_D >$ 10 μM). Nevertheless, the adaptability required for applications of synthetic multifunctional pores as enzyme sensors[23] was confirmed for KH pore **1** by the differences found in the molecular recognition of poly-L-glutamate, ATP, and PTS.

Molecular recognition by KH pore hosts **1** not only blocked the efflux of large organic anions (ANTS) and/or cations (DPX) through KH pore hosts **1**, it also hindered the translocation of small inorganic cations (potassium) and anions (chloride). The macroscopic conductance of planar EYPC bilayers doped with pore hosts **1** was strongly reduced in the presence of increasing concentrations of HPTS **6** (Figure 5B). The high $K_D = 190 \pm 10$ μM obtained from Hill analysis of the dose response curve at $V = +100$ mV was consistent with the poor blockage observed with PTS in spherical bilayers. This comparably poor host−guest interaction with KH pore **1** was clearly different from HPTS blockage of HH pore **2** ($K_D = 0.2$ μM), RH pore **3** ($K_D = 3.0$ μM), and RH pore **4** ($K_D = 3.0$ μM) as well as the $K_M = 0.6$ μM obtained for the esterolysis of AcPTS **5** by KH catalyst **1** (see below). The high Hill coefficient $n = 4.9 \pm 1.0$ found for HPTS blockage of pore **1** supported the view that multiple guest binding may be required to block the unusually large KH pore **1**, whereas high-affinity binding of one pyrene-1,3,6-trisulfonate substrate at the inner barrel surface may suffice for catalysis.

Rigid-Rod β-Barrels with Internal KH Dyads as Catalysts. The catalytic activity of rigid-rod β-barrel **1** was evaluated using AcPTS **5** as established model substrate (Figure 2).[14,21,24] Esterolysis of substrate **5** was continuously detectable by monitoring the increase in the fluorescence emission of the product HPTS with time.[14,21] The dependence of the esterolytic activity of rigid-rod β-barrel **1** on pH was comparable to the pH profile of rigid-rod β-barrel **1** as pore (Figure 6A, filled circles, versus Figure 3A). The pH profile of KH catalyst **1** was similar to that of HH catalyst **2**.[14] For complete comparison, the pH profile of RH catalyst **3** was determined (Figure 6A, empty circles). Different from KH and HH catalysts **1** and **2**, the catalytic activity of RH catalyst **3** did not decrease between pH 5.5 and pH 6.8 (above pH 6.8, precipitation was observed). This suggested that the loss in catalytic activity with increasing pH may originate from neutralization of internal, proximal histidines (**2**, intrinsic $pK_a = 6.0$) and lysines (**1**, intrinsic $pK_a = 10.5$) but not arginines (**3**, intrinsic $pK_a = 12.5$). This reduction of the number of cations at the inner barrel surface with increasing pH may either reduce the interaction with the anionic substrate **5** or—according to the ICR model[20]—destabilize the active suprastructure.

Direct experimental evidence that the active catalysts are tetrameric barrel-stave supramolecules (rather than monomeric peptide−*p*-octiphenyl conjugates) was obtained, for the first time, with the c_M profile of catalyst **1** (Figure 6B, filled circles). The nonlinear dependence of the initial velocity of product formation on the concentration of monomeric peptide−*p*-octiphenyl conjugate $\mathbf{1^m}$ gave a Hill coefficient $n = 3.7 \pm 0.2$ that was indicative for unstable tetramers as active supramolecular catalysts (Figure 6B, solid). The stability of rigid-rod β-barrel **2** known from pore characterization ($n = 1.0$, Figure 1) was reflected in the c_M profile for catalysis ($n = 0.9 \pm 0.1$,

(28) (a) Smart, O. S.; Breed, J.; Smith, G. R.; Sansom, M. S. P. *Biophys. J.* **1997**, *72*, 1109−1126. (b) Cruickshank, C. C.; Minchin, R. F.; Le Dain, A. C.; Martinac, B. *Biophys. J.* **1997**, *73*, 1925−1931.

(29) Applied to host−guest chemistry, the meaning of the Hill coefficient n (or sometimes h) can be more complex as well and include cooperativity beyond the number n of guests bound per host. Compare, e.g.: Connors, K. A. *Binding Constants*; John Wiley & Sons: New York, 1987; pp 59−101.

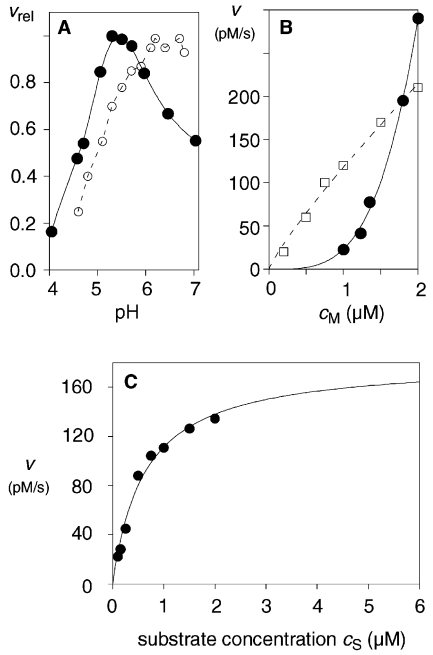

Figure 6. Dependence of supramolecular catalysis by rigid-rod β-KH barrel **1** on pH (A), c_M (B), and c_S (C) (filled circles) in comparison with HH catalyst **2** (empty squares) and RH catalyst **3** (empty circles). The initial velocity $v_{(rel)}$ of product formation was measured following the increase in HPTS emission after addition of monomers $\mathbf{1^m}$ (filled circles: (A) 5.0 μM, 1.0 μM AcPTS **5**; (B) pH 5.5, 1.0 μM **5**; (C) 1.5 μM, pH 5.5), $\mathbf{3^m}$ (empty circles: (A) 0.25 μM, 7.0 μM **5**), or $\mathbf{2^m}$ (empty squares: (B) pH 5.5, 1.0 μM **5**) in 10 mM MES, 100 mM KCl. Curves were fitted to the Hill ((B) solid, $n = 3.7 \pm 0.2$; dotted, $n = 0.9 \pm 0.1$) and Michaelis−Menten equations ($K_M = 0.6 \pm 0.1$ μM, $v_{MAX} = 181 \pm 11$ pM/s).

Figure 6B, dotted). Interpretation of the tetrameric, unstable and "invisible" KH catalysts **1** as aqueous rigid-rod β-barrel prepores with a suprastructure similar to that of the KH pores **1** in the bilayer was supported by identical stoichiometry and thermodynamic instability (Figure 1). Supramolecular catalyst and supramolecular pore were, therefore, in all likelihood the same multifunctional rigid-rod β-barrel **1**. The remarkable consistency throughout the characteristics of multifunctional pores **1**−**3** suggested that this conclusion applies for the more stable pores **2** and **3** as well, although direct evidence for supramolecular function from c_M profiles was not available in these cases because of higher thermodynamic stability.

Variation of substrate concentration at constant catalyst concentration and pH revealed the Michaelis−Menten constant $K_M = 630 \pm 97$ nM (Figure 6C). This remarkable substrate recognition by KH catalyst **1** was as for HH catalyst **2** ($K_M = 700$ nM)[14] and 10 times better than for RH catalyst **3** ($K_M = 6.1$ μM).[24] The $k_{cat} = 0.03$ min^{-1} of KH catalyst **1** was, however, clearly below that of HH catalyst **2** ($k_{cat} = 0.13$ min^{-1}) and RH catalyst **3** ($k_{cat} = 0.24$ min^{-1}). This unusually low k_{cat} was consistent with the endergonic self-assembly of the supramolecular catalyst **1** identified with a nonlinear c_M profile (Figure 6B). Specifically, the assumption of a $k_{cat}' \approx 0.18$ min^{-1} for an active supramolecule like that of HH and RH catalysts suggested $c_B' \approx v_{MAX}/k_{cat}' = (k_{cat}c_M/4)/k_{cat}' = 62.5$ nM as the effective concentration of KH catalyst **1** at $c_M = 1.5$ μM. This result implied $c_M' = c_M - 4c_B' \approx 1250$ nM as excess monomer under these conditions. These effective monomer and tetramer concentrations corresponded to an approximate monomer/barrel ratio of $c_M'/c_B' = 20$. The resulting $K_D = (c_M')^4/c_B' = 39$ μM^3 for the active supramolecule **1** was compatible with endergonic self-assembly at the concentrations relevant for multifunctionality.

The $K_M = 0.6$ μM for esterolysis of AcPTS **5** by KH catalyst **1** was more than 2 orders of magnitude lower than the $K_D = 190$ μM for the blockage of KH pore **1** in planar bilayers by HPTS. This is the first time that such a difference between molecular recognition and catalysis was observed with multifunctional rigid-rod β-barrels. Although the origin of this difference is unknown, its coincidence with an exceptionally large inner pore diameter and an exceptionally high Hill coefficient for HPTS blockage ($n = 4.9$) may be more than accidental. Indeed, molecular simulations supported the view that the origin of the high conductance of pore **1** may be not only the absence of immobilized internal counteranions but also a swelling of the rigid-rod β-barrel tetramer in response to high internal charge repulsion. Above results suggested that the structure of the inclusion complex accounting for pore blockage may be different from that accounting for catalysis. The possibility of different orientations for included pyrene-1,3,6-trisulfonates is illustrated in modeling studies below (Figure 7B,C). Alternatively, it was conceivable that multiple pyrene-1,3,6-trisulfonate binding may be needed for pore blockage, whereas single AcPTS binding may suffice for catalysis. This explanation was supported by $n = 4.9$ for HPTS blockage.[29]

Molecular Modeling of Multifunctional Rigid-Rod β-Barrel with Internal KH Dyads. The demonstrated experimental inaccessibility to structural information on rigid-rod β-barrel pore **1** identified molecular modeling as a unique resource for insights on supramolecular multifunctionality at the molecular level. Therefore, rigid-rod β-barrel **1** was constructed using Maestro modeling software.[30] Imitating the synthesis of barrel **1** (Scheme 1), four peptide−*p*-octiphenyl conjugates $\mathbf{1^m}$ were constructed first and then assembled to give the supramolecular tetramer. Taking counteranion-mediated charge neutralization and the ICR model into account, only every second internal lysine was protonated before preliminary geometry optimization using the MMFF94 force field[31] as implemented in the MacroModel package.[32]

The energy-minimized rigid-rod β-barrel **1** had a height of 32.4 Å, a mean backbone-to-backbone diameter of 35 Å, and a minimal inner van der Waals diameter of 16.2 Å (Figure 7A). The inner pore diameter was in excellent agreement with the experimental Hille diameter $d_{Hille} \approx 12$ Å. β-Barrel **1** had an *M*-helical twist of 20°. In a hypothetical rigid-rod β-barrel of infinite length, this nearly negligible helicity would give rise to a helix with 144 β-strands per turn, i.e., a helical pitch of about 58 nm corresponding to 18 barrels on top of each other. The preferred biphenyl torsion angles $\omega \approx 123°$ in the *p*-octiphenyl staves accounted for the circular, truly barrel-like appearance of tetramer **1** viewed from the top. Preliminary results indicated that uniform isomerization to energetically conceivable biphenyl torsions $\omega \approx 57°$—in response to, e.g., reduced internal charge repulsion—would produce contracted conformers with drastically reduced inner diameter. Possible

(30) *Maestro 4.1*; Schrödinger Inc.: Portland OR, 2001.
(31) (a) Halgren, T. A. *J. Comput. Chem.* **1996**, *17*, 490−641. (b) Halgren, T. A. *J. Comput. Chem.* **1999**, *20*, 720−748.
(32) (a) *MacroModel 7.0*; Schrödinger, Inc.: Portland OR, 1999. (b) Mohamadi, F.; Richards, N. G. J.; Guida, W. C.; Liskamp, R.; Lipton, M.; Caufield, C.; Chang, G.; Hendrickson, T.; Still, W. C. *J. Comput. Chem.* **1990**, *11*, 440−467.

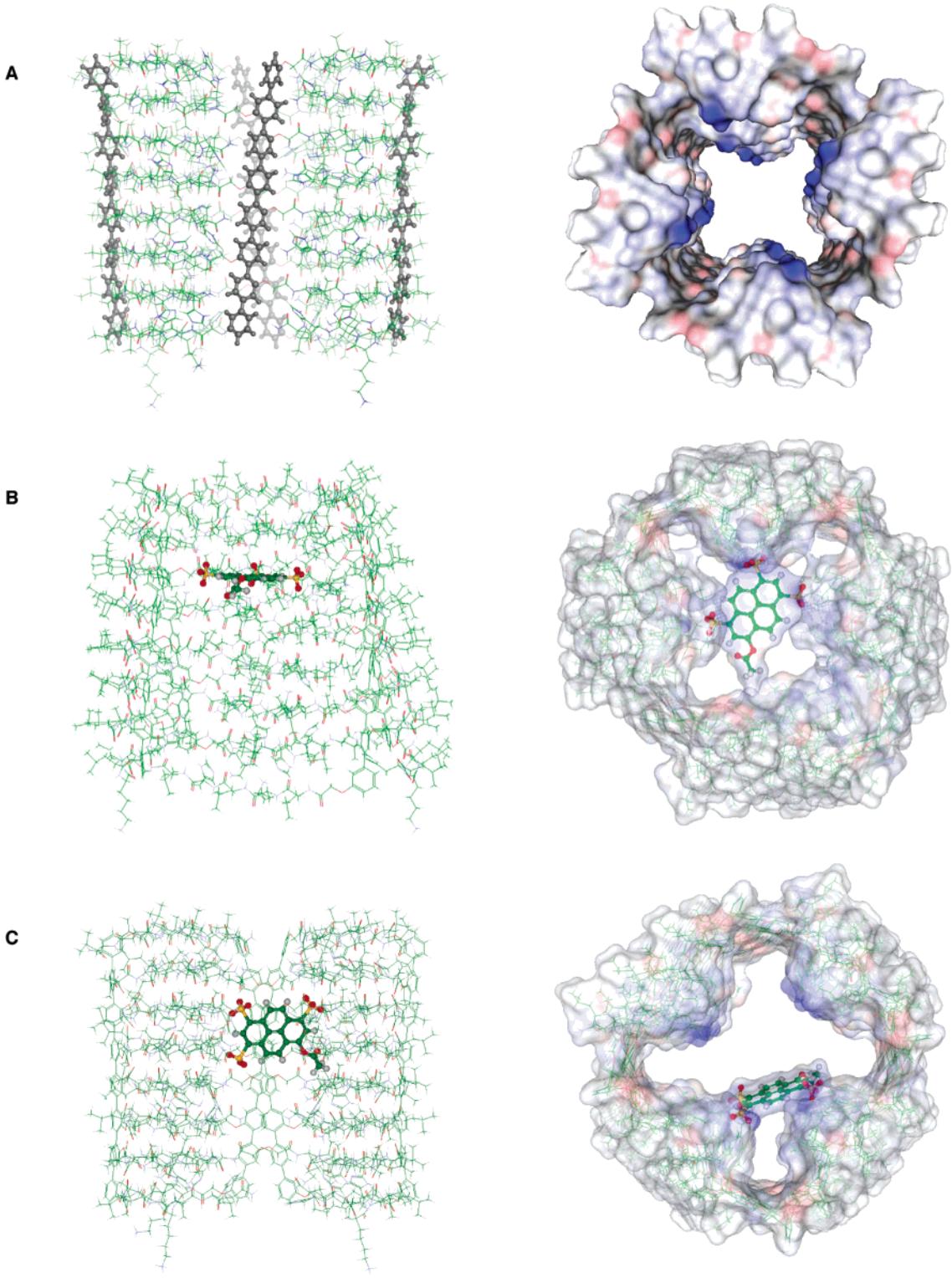

Figure 7. Three-dimensional structure optimized by MacroModel (MMFF94) of rigid-rod β-barrel **1** (lysine protonation 50%, histidine protonation 0%) in side view (left) and axial view (right) without guests (A) and with AcPTS (sulfonate protonation 0%) bound perpendicular (B, $\mathbf{1} \supset \mathbf{5}^{\perp}$) and parallel to the long barrel axis (C, $\mathbf{1} \supset \mathbf{5}^{=}$). Side views are wire presentations (O, red; N, blue; C, green; H, gray) with *p*-octiphenyls (A, black) and AcPTS highlighted in ball-and-stick (B, C: O, red; S, yellow; C, green; H, gray). Axial views show electrostatic potentials mapped onto solvent-accessible surfaces (blue, electron-poor; red, electron-rich) with (B, C) semitransparent surface to reveal barrel and AcPTS in wire and ball-and-stick presentation, respectively.

strain from the suppressed, intrinsic β-sheet helicity[33] may account for some local asymmetries in barrel **1**; refined simulations will be needed to evaluate their relevance.

Possible inclusion complexes of AcPTS **5** within supramolecular catalyst **1** were simulated by docking of the substrate between the first and second β-sheet hoops with the pyrene plane either perpendicular (i.e., inclusion complex $\mathbf{1} \supset \mathbf{5}^{\perp}$, Figure 7B) or parallel to the long barrel axis ($\mathbf{1} \supset \mathbf{5}^{=}$, Figure 7C). Before docking, AcPTS was optimized with the density functional

(33) (a) Richardson, J. S. *Nature* **1977**, *268*, 495−500. (b) Flower, D. R. *FEBS Lett.* **1994**, *344*, 247−250. (c) Nagano, N.; Hutchinson, E. G.; Thornton, J. M. *Protein Sci*. **1999**, *8*, 2072−2084 (see also ref 13).

theory (DFT)[34] and B3LYP/6-31G* method.[35] After this initial optimization, substrate **5** was frozen in the DFT geometry. In other words, substrate **5** was considered as the rigid body during the optimizations of complex **1** ⊃ $\mathbf{5}^{\perp}$ by MMFF94 force field. To obtain complex **1** ⊃ $\mathbf{5}^{\perp}$, DFT-optimized AcPTS was docked at the barrel entrance, spanning the interior to interact with charged residues from opposing β-sheets. During optimization, the substrate **5** moved into the pore to end up 10.8 Å from the channel entrance (Figure 7B). Asymmetric barrel contraction reduced the minimal internal diameter on the substrate side from 16.2 to 10.4 Å. This asymmetric barrel contraction into a cone-shaped conformation originated from complete inward extension of the internal lysine residues to reach the substrate for ion pairing and multiple, bilateral H-bonding between two ammonium cations per sulfonate anion (average N−H···O distance = 2.6 Å). These changes provided a compelling illustration for likely contributions from supramolecular adaptability and guest templation to pore blockage.

During optimization of **1** ⊃ $\mathbf{5}^{=}$, vertical movement of B3LYP/6-31G* optimized substrate **5** from the barrel entrance toward the barrel center as with **1** ⊃ $\mathbf{5}^{\perp}$ coincided with a lateral displacement from one β-sheet surface to the interface between adjacent β-sheets (Figure 7C). Inclusion complex **1** ⊃ $\mathbf{5}^{=}$ exhibited complementary characteristics compared to **1** ⊃ $\mathbf{5}^{\perp}$ with regard to negligible barrel deformation and poor blockage. This complementarity confirmed that molecular recognition within synthetic multifunctional pores may occur with or without a strong influence on molecular translocation (i.e., blockage), whereas catalysis appeared possible in both cases (i.e., histidine−carbonyl distances around 5 Å compatible with nucleophile or base catalysis with possible electrophile activation and transition-state stabilization by ammonium cations near the carbonyl oxygen). Much room left by these initial simulations is currently explored with emphasis on the impact of biphenyl torsions, internal charge repulsion, guest templation, guest diversity, solvents, bilayer membranes, and molecular dynamics on barrel structure. Particular emphasis is on multiple guest/substrate binding to ultimately simulate synthetic catalytic pores (i.e., substrate transformation during transmembrane translocation),[17] including the recent concept that blocker efflux through blocked pores may translate the mechanism of selectivity of biological ion channels[36] to organic chemistry within synthetic multifunctional pores.[37]

(34) Frisch, M. J.; Trucks, G. W.; Schlegel, H. B.; Scuseria, G. E.; Robb, M. A.; Cheeseman, J. R.; Montgomery, J. A., Jr.; Vreven, T.; Kudin, K. N.; Burant, J. C.; Millam, J. M.; Iyengar, S. S.; Tomasi, J.; Barone, V.; Mennucci, B.; Cossi, M.; Scalmani, G.; Rega, N.; Petersson, G. A.; Nakatsuji, H.; Hada, M.; Ehara, M.; Toyota, K.; Fukuda, R.; Hasegawa, J.; Ishida, M.; Nakajima, T.; Honda, Y.; Kitao, O.; Nakai, H.; Klene, M.; Li, X.; Knox, J. E.; Hratchian, H. P.; Cross, J. B.; Adamo, C.; Jaramillo, J.; Gomperts, R.; Stratmann, R. E.; Yazyev, O.; Austin, A. J.; Cammi, R.; Pomelli, C.; Ochterski, J. W.; Ayala, P. Y.; Morokuma, K.; Voth, G. A.; Salvador, P.; Dannenberg, J. J.; Zakrzewski, V. G.; Dapprich, S.; Daniels, A. D.; Strain, M. C.; Farkas, O.; Malick, D. K.; Rabuck, A. D.; Raghavachari, K.; Foresman, J. B.; Ortiz, J. V.; Cui, Q.; Baboul, A. G.; Clifford, S.; Cioslowski, J.; Stefanov, B. B.; Liu, G.; Liashenko, A.; Piskorz, P.; Komaromi, I.; Martin, R. L.; Fox, D. J.; Keith, T.; Al-Laham, M. A.; Peng, C. Y.; Nanayakkara, A.; Challacombe, M.; Gill, P. M. W.; Johnson, B.; Chen, W.; Wong, M. W.; Gonzalez, C.; Pople, J. A. *Gaussian 03*, Revision A.1; Gaussian, Inc.: Pittsburgh, PA, 2003.
(35) (a) Becke, A. D. *Phys. Rev. A* **1988**, *38*, 3098−3100. (b) Lee, C.; Yang, W.; Parr, R. G. *Phys. Rev. B* **1988**, *37*, 785−789. (c) Miehlich, B.; Savin, A.; Stoll, H.; Preuss, H. *Chem. Phys. Lett.* **1989**, *157*, 200−206.
(36) (a) Doyle, D. A.; Cabral, J. M.; Pfuetzner, R. A.; Kuo, A.; Gulbis, J. M.; Cohen, S. L.; Chait, B. T.; MacKinnon, R. *Science* **1998**, *280*, 69−77. (b) MacKinnon R.; Cohen, S. L.; Kuo, A.; Lee, A.; Chait, B. T. *Science* **1998**, *280*, 106−109. (c) Roux, B.; MacKinnon, R. *Science* **1999**, *285*, 100−102.
(37) Ronan, D.; Sordé, N.; Matile, S. *J. Phys. Org. Chem.*, in press.

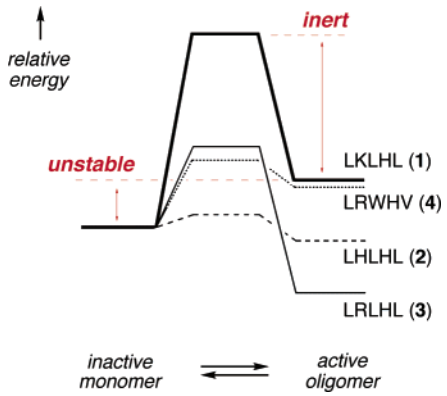

Figure 8. Notional energy diagrams summarizing the thermodynamic and kinetic stabilities achieved with synthetic multifunctional pores **1**−**4**. Unstable and inert pores such as **1** are suggested to be "ideal" in practice.

Conclusions

Rigid-rod β-barrels **1** with internal lysine−histidine dyads complete a comprehensive collection of synthetic multifunctional pores that now covers all possible combinations of thermodynamic and kinetic stabilities (Figure 8). The power of bacterial pore-forming toxins underscores that endergonic self-assembly from hydrophilic monomers into inert synthetic multifunctional pores **1** is ideal for practical sensing applications because too stable pores (such as **2** and **3**) tend to precipitate rather than to partition into bilayer membranes, whereas too labile pores (such as **2** and **4**) are useless as single-molecule sensors.

One attractive characteristic resulting from the rationally designed inertness of rigid-rod β-barrels **1**, on one hand, is their long lifetime as single, multifunctional and large, i.e., high-conductance, pores. Attractive characteristics resulting from the instability of rigid-rod β-barrels **1**, on the other hand, include access to unprecedented experimental evidence for supramolecular multifunctionality, expressed in $n = 4.0$ for pore **1** and $n = 3.7$ for catalyst **1**. Experimental support is provided for minimal internal counterion immobilization and, as a consequence, maximal internal charge repulsion to account for the large inner diameter of pore **1** ($d \approx 12$ Å). Multiple binding of several small (HPTS, $K_D = 190$ μM, $n = 4.9$) but not single large blockers (polyglutamate, $K_D \leq 105$ nM, $n = 1.0$) may be required to "fill" this large, swollen internal space of high-conductance KH pore **1**, whereas molecular recognition of single small substrates may suffice for catalysis (AcPTS, $K_M = 0.6$ μM). Supported by preliminary results from molecular modeling, we conclude that the multifunctional rigid-rod β-barrel pores **1** reported herein offer a superb platform to study chemical processes that take place within their confined, oriented, inert, and functionalized internal nanospace.

Acknowledgment. We thank B. Baumeister for experimental assistance, D. Jeannerat, A. Pinto, and J.-P. Saulnier for NMR measurements, F. Gülaçar for assistance with ESI MS, H. Eder for elemental analyses, two reviewers for helpful suggestions, and the Swiss NSF for financial support (200020-101486 and National Research Program "Supramolecular Functional Materials" 4047-057496).

Supporting Information Available: Experimental Section (PDF). This material is available free of charge via the Internet at http://pubs.acs.org.

JA0481878